Water Practice & Technology

IWA PUBLISHING

Water Practice & Technology Vol 17 No 5, 1099 doi: 10.2166/wpt.2022.042

Water purification using an eco-friendly adsorbent

Maali Alamjad Hassan* and Isra'a Sadi Samaka

Department of Environmental Engineering, College of Engineering, University of Babylon, Babylon, Iraq
*Corresponding author. E-mail: eng.israa.sadi@uobabylon.edu.iq

ABSTRACT

The literature has proved the high efficiency of activated carbon in removing a wide range of pollutants from water; however, the high cost of industrial types of activated carbon is one of the barriers to the wide application of this efficient adsorbent. Therefore, this study aims at the development of a new type of activated carbon from the Schanginia/sp plant (Schanginia activated carbon (SAC)) and the possibility of using it as a biosorbent for the removal of methylene blue dye (MBD) from water. The SAC was subjected to characterisation analysis, including the surface area (S_{BET}), Fourier-transform infrared spectroscopy (FTIR), scanning electron microscope (SEM), and statistical parametric mapping (SPM) before using it to remove the MBD. Furthermore, the efficacy of SAC was investigated in batch experiments, taking into account the effects of several experimental factors, namely pH of the solution, contact duration, SAC dose, and MBD concentration. The results showed the maximum uptake of MBD was 33.34 mg/g, and the Langmuir model is suitable to reproduce the optimum biosorption. In conclusion, the obtained results proved the applicability of SAC for the removal of MBD from water.

Key words: activated carbon, biosorption, dye, Langmuir model

HIGHLIGHTS

- A new type of activated carbon was made from natural sources.
- The effects of operating parameters was studied.
- Characterisation of the adsorbent was conducted using SBET, FTIR, SEM, and SPM.
- The new adsorbent removed 33.34 mg/g of dyes in water.

1. INTRODUCTION

It is an undeniable fact the planet of Earth is facing a wide range of serious environmental problems, ranging from climate change (Salah *et al.* 2018, 2022) to air pollution (Al-Sareji *et al.* 2021; Grmasha *et al.* 2021) and production of solid wastes (Abdulredha *et al.* 2017). However, water pollution is the most significant dilemma due to the limited sources of fresh water on this planet (Al-Hashimi *et al.* 2021; Arab *et al.* 2022). The increasing utilisation of dyes in many industries, such as textile, pharmaceutical, food, paper, and leather, has resulted in serious environmental damage (Yagub *et al.* 2014; Hashim *et al.* 2019). Coloured effluents can harm water sources as dyes have a considerable solubility in water, even in low concentrations. In addition, dyes are undesirable in drinking water, minimise sunlight, and reduce photosynthesis and oxygenation in water bodies (Albadarin *et al.* 2014; Omran *et al.* 2019). Dye pollution of water bodies may be toxic to aquatic creatures, preventing organismal degradation and disrupting biological cycles. Furthermore, toxic dyes induce skin irritation, allergic dermatitis, genetic mutations, and cancer risk (Chung 2016). Dyes' removal from aqueous solutions is constrained by several factors, including high prices, the generation of hazardous substances, and high energy requirements. So to reduce dye concentration in wastewater, cost-effective, efficient, and ecologically friendly technology must be developed (Tahir *et al.* 2016; Abdulhadi 2022). Different approaches might be used to remove dye from coloured effluents. Biodegradation, solvent extraction, ion exchange, oxidation, and adsorption are some of the processes involved (Sivarajasekar & Baskar 2015; Sharma & Kaur 2018; Hashim *et al.* 2021b). For example, the electrocoagulation method is currently in use for dye removal from solutions (Emamjomeh *et al.* 2020; Abdulhadi *et al.* 2021; Hashim *et al.* 2021a). Hashim *et al.* (2019) used an electrocoagulation cell to remove black reactive dyes from water under different experimental conditions and found the removal efficiency reached 96%. Removal of dyes using plants is another common method nowadays; for example, Karaghool *et al.* (2022) used sweet basils to remove a textile dye from water. Although the sweet basils removed

93% of 25 mg/L of the dye, the required time was very long (about ten days). Adsorption is one of the most attractive methods for dye removal because it is simple, dependable, ecologically safe, and cost-effective. Activated carbon, which is described as a carbonaceous solid with a high surface area and substantial microporosity, has been used to filtrate dirty water for a few decades (Soonmin 2018). It is also being utilised as a conventional adsorbent more regularly (Dias *et al.* 2007). Artificially activated carbon, on the other hand, is prohibitively expensive. As a result, several studies have focused on the production of activated carbon from a variety of low-cost materials, including orange peel (Teka & Enyew 2014), solid pineapple waste (Mahamad *et al.* 2015), palm shell waste (Wong *et al.* 2016), and peanut shell (Georgin *et al.* 2016). In this context, this research aims to check the usability of a natural plant-activated carbon to remove methylene blue dye (MBD) from the aqueous medium in batch mode.

2. MATERIALS AND METHOD

2.1. Biosorbent formulation

The biosorbent employed in this study was activated carbon produced from a native Iraqi plant (Schanginia/sp.) (SAC). This plant may be found in many locations in Iraq. The activation of the corresponding material by carbonisation was used to produce activated carbon. The plant was chopped into small pieces and carbonised for one hour at 250 °C in a muffle furnace (Thermo Scientific TY408X-2A, USA); the furnace was heated first to 250 °C before starting the carbonisation process, which means the plant pieces were subjected to a temperature of 250 °C for one hour. The level and duration of heating were determined through a series of tests with various degrees and intervals. As the level of heating and period were raised, the plant was totally carbonised to ash. The activated carbon was rinsed many times with distilled water before being baked in an electric oven at 100 °C to remove any excess moisture and stored in a desiccator. The biosorbent was finally crushed and sieved using a 100 mesh sieve.

2.2. Characterisations of manufactured biosorbent

The BET surface area of SAC was calculated using nitrogen adsorption-desorption isotherms acquired at a relative pressure of 0.35 p/p^o using a Thermo Finnegan analyser (Qsurf-9600, USA). Different assays were conducted before and after the biosorption procedure to validate the biosorption of MBD onto SAC. Using a KBr tablet, Fourier-transform infra red (FTIR) spectroscopy (SHIMADZU, IRPrestige-21, Japan) was used to detect the presence of functional groups on the SAC surface in the range of 4,000–400 cm^{-1}. The changes in SAC surface and form before and after MBD removal were studied using scanning electron microscopy (SEM) (TESCAN, Mira3, France), which produces high-resolution images and elemental analysis using energy dispersion spectroscopy (EDS). SPM was used to investigate the topography of SAC (SPM AA300, Advanced Angstrom Inc., USA, with contact style of AFM). The pH value when the end and the initial pH are the same and the biosorbent surface charge is neutral at this value (point zero charges, pH_{pzc}) is an essential feature for determining which ionic types may be absorbed by the biosorbent at the desired pH. The pH_{pzc} of SAC is calculated using the batch equilibrium approach, as described before (Mohseni-Bandpi *et al.* 2016). SAC (0.5 g) was put in conical flasks containing 50 ml 0.1M NaCl solution. The main pH (pH_i) values (2–9) were arranged using a 0.1 M NaOH or HCl solution. After that, the suspensions were agitated for 24 hours at 150 rpm. After that, SAC was separated, and the solution's pH value was measured. The pH_{pzc} is calculated by graphing the pH vs pH_i curve from the point of interception zero.

2.3. Batch experiments of biosorption

All MBD biosorption tests on SAC were carried out in batch mode at room temperature, using several conical flasks with capacities of 250 and 100 ml. It was vital to observe the effects of operational parameters on MBD biosorption to identify the ideal conditions for MBD removal and to get a larger number of equilibrium data suitable for determining the interacting material activity and biosorption isotherm. Therefore, the influence of pH of MBD solution, contact time, biosorbent mass, and starting MBD concentration were investigated. To investigate the effects of solution pH and contact duration, 50 mg/l of MBD solution was agitated with 0.8 g of SAC at 250 rpm for 120 minutes with varied pH values (2–10). The impact of SAC dosage with 50 mg/l dye concentration at 250 rpm, optimal contact time with pH determined from previous tests, was investigated using SAC mass ranging from 0.1 to 1.5 g/100 ml MBD solution. By adding the optimal dosage of SAC and the best pH value at equilibrium time, the impact of the primary concentration of dye on the biosorption capacity of SAC

was observed using various concentrations of MBD in the range of 10–100 mg/l. These findings were also based on the examination of isotherm investigations. At the end of each experiment, a solution sample was obtained from each flask and filtered for testing with a UV-vis spectrophotometer with a double beam (UV-vis-6800 JENWAY) at maximum wavelength $\lambda_{max} = 664$ nm to measure the residual dye concentration. Equations (1) and (2) were used to calculate the amount of MBD biosorbed (q_e, mg.g^{-1}) and the SAC's biosorption effectiveness ($R\%$) (Etim 2019).

$$q_e = (C_o - C_e)/M*V \quad (1)$$

$$(R\%) = (C_o - C_e)/C_o*100\% \quad (2)$$

where C_o and C_e (mg/l) signify the concentrations of MBD in the liquid phase at primary and equilibrium, M (g) denotes the amount of biosorbent utilised, and V (l) is the dye solution volume.

2.4. Chemical structure

In this research, analytically ranked reagents were employed. The adsorbate, MBD (Basic blue 9), was obtained from Sigma Aldrich. [7-(Dimethylamino) phenothiazine-3-ylidene]- chloride of dimethylazanium is the IUPAC systemic name for this compound, CI 52,015, molecular mass 319.85 with a maximum absorption wavelength of 664 nm; molecular formula = $C_{16}H_{18}N_3ClS$. Batch mode was used to research MBD biosorption. The pH was regulated with a 0.1 M solution of NaOH and HCl.

3. RESULTS AND DISCUSSION

3.1. Characterisations of SAC

EDS analysis was used to get the elemental analysis of SAC, which is presented in Table 1.

Table 1 | SAC elemental analysis (% W/W)

Biosorbent	C	O	N	H	S	Other contents plus loss of ignition (LOI)
SAC	69.52	12.36	1.93	6.24	1.3	8.65

The SAC sample has an extremely high carbon concentration compared to other elements. As a result, it can be concluded that carbon is the main component in the sample, indicating that it is carbonaceous and suitable for adsorption. S had a very low extent, indicating that just a few contaminants were present. Table 2 lists the various physicochemical features of SAC.

Table 2 | SAC's physiochemical properties

Property	Value
Specific surface area, S_{BET} ($m^2\ g^{-1}$)	27.92
Moisture content %	0.3
Bulk density (g/ml)	0.356
Point zero charge (pH_{pzc})	4.4

FTIR is a spectroscopy method used to evaluate functional groups located on the surface of biosorbents that may be involved in MBD interactions and biosorption (Giannakoudakis *et al.* 2018). Figure 1(a) and 1(b) show the FTIR spectra of SAC in the 400–4,000 cm^{-1} range before and after MBD removal to explain the positions of active sites of these functional groups and the shifting of their locations after MBD removal. The presence of a significant number of IR bands, which appear to be crucial to many functional groupings, in agreement with their own wavelengths, demonstrates the complex character of SAC in Figure 1(a) (cm^{-1}). The –OH stretching vibrations of the hydrogen-bound hydroxyl group of polymeric substances such as carboxylic acids, phenols, and alcohols in the group of pectin and cellulose located on the surface of the biosorbent are

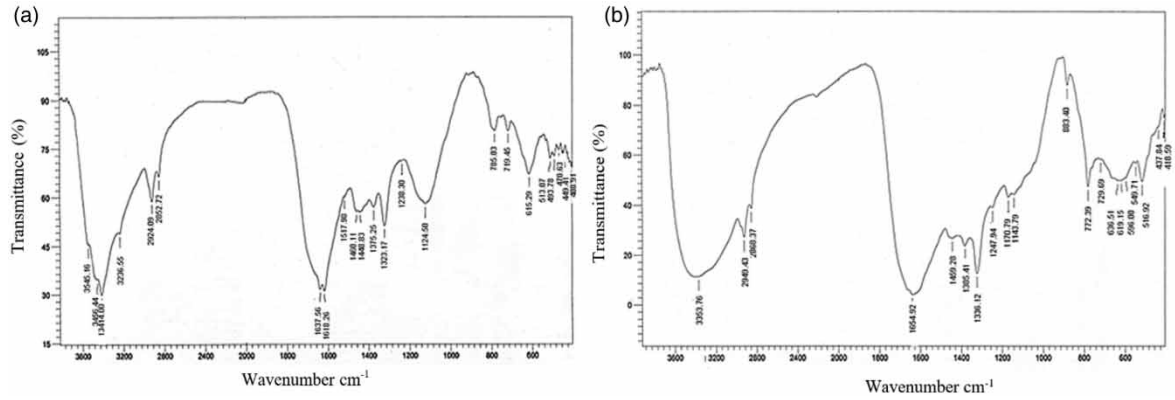

Figure 1 | Spectra of FTIR of SAC (a) before MBD biosorption and (b) after MBD biosorption.

characterised by high and wide absorption peaks in the range of 3,414–3,236.55 cm^{-1}. The beneficial oxygen groups on the surface of the SAC significantly boost its hydrophilic properties and serve as binding sites for contaminating organic molecules (Chen *et al.* 2015). In this area, the –NH asymmetric stretching of amino groups was also seen (Latif *et al.* 2019). The peaks at 2,924.09 and 2,852.72 cm^{-1} are symmetric and asymmetric, respectively, for the C-H stretching vibrations of aliphatic acids (Latif *et al.* 2019). The peaks at 1,637.56 and 1,618.28 cm^{-1} correspond to C = O stretching associated with carboxyl organic groups and bend vibrating of the functional group –OH, respectively (Silva *et al.* 2019). The peak at 1,460.11 cm^{-1} reveals the stretching vibrations of aromatic C = C groups in aromatic rings (Sever *et al.* 2019). The –COO- symmetric stretching vibrations and C-N stretching vibrations have maxima at 1,375.25 and 1,323.17 cm^{-1}, respectively (Das *et al.* 2020). N-O stretching vibrations of aliphatic amines (Ansari *et al.* 2016). IR bands show stretching vibrations of C-O and C-O-C groups of carboxylic acids, phenols, alcohols or esters are shown by IR bands at 1,000–1,300 cm^{-1} (Jawad *et al.* 2018). C-N stretching vibrations are represented by the peaks at 785.03 and 719.45 cm^{-1} (Zhang *et al.* 2013). Furthermore, the presence of alkyl halide compounds with a C-Br (stretched vibration) bond is indicated by the peaks below 700 cm^{-1} (Kanthasamy *et al.* 2020). As shown in Figure 1(a), the SAC surface before MBD biosorption is rich in hydroxyl, carbonyl, and carboxylic groups, which act as proton donors to bind cationic MBD as other medium and weak functional groups that contribute to dye removal. New peaks were formed, which indicates the possible involvement of alkyne and ester groups in the adsorption process during the biosorption of MBD onto the surface of the biosorbent surface (Figure 1(b)) (Rao 2021). These differences in peaks before and after adsorption suggested that these functional groups play a major role in MBD biosorption via electrostatic interaction with positively charged MBD molecules. H-bonding interactions between H atoms on the SAC surface and N atoms in the MBD structure are also part of the biosorption mechanism. Other studies have given similar reasons for MBD biosorption employing coal-activated carbon (Jawad *et al.* 2019).

The SEM method was used to give pictures at different magnifications for investigating the morphology of the SAC surface before and after MBD biosorption to explore the textural morphology of the surface. Before MBD biosorption, the SEM images (Figure 2(a)) revealed an uneven structure with cracks and many non-homogeneous ravines formed on the SAC surface, which give a significant surface area for dye removal. Several noticeable changes occurred after MBD biosorption (Figure 2(b)), such as a smooth surface with glossy and white patches. The appearance of white patches and dots could indicate that some of the dye was removed through physical adsorption (Oliva *et al.* 2018). Furthermore, the surface of the SAC seemed to be coated in a thick layer of sediments due to absorbed MBD completely filling the pores. This observation was supported by the literature (Jabar *et al.* 2020).

As shown in Figure 3(a) and 3(b), the SPM test was used to characterise and assess the topography of the SAC before and after MBD biosorption. According to Figure 3(a), the SAC before MBD biosorption exhibits an uneven and deformed surface with considerable strata of uneven heterogeneous holes, indicating a high possibility of MBD molecules being absorbed. On the other hand, Figure 3(b) shows a flatter surface with reduced pore structures following MBD biosorption, implying biosorption and establishment of MBD molecules by the readily reachable pore surrounding regions of the SAC surface (Jawad *et al.* 2018). Table 3 summarises the most important findings from this study.

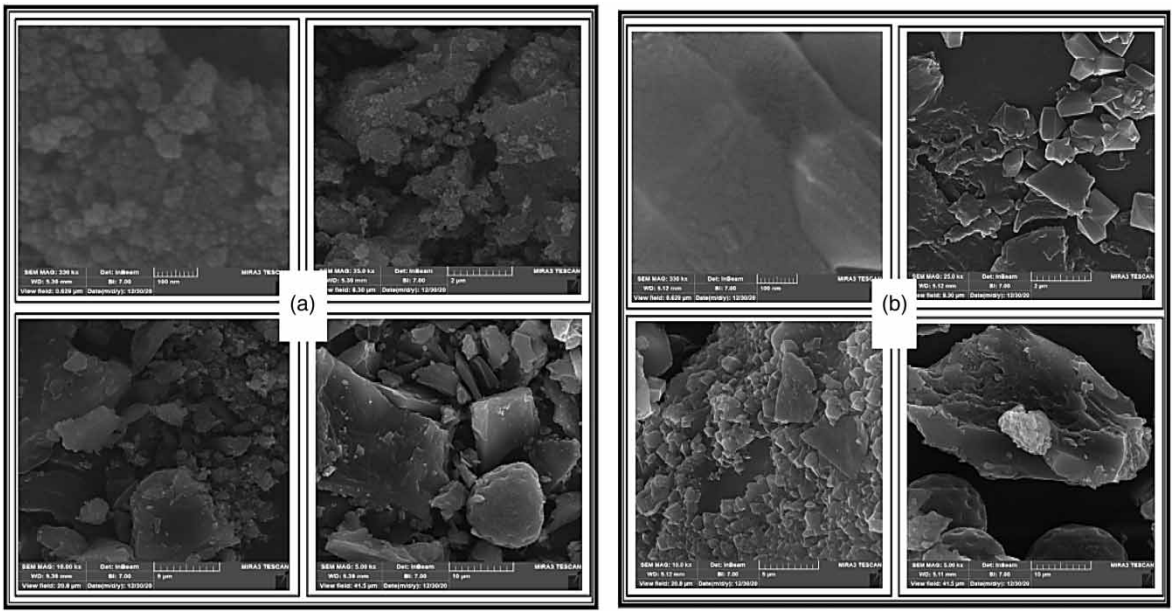

Figure 2 | SEM micrograph images of SAC at different magnifications: (a) before MBD biosorption (b) after MBD biosorption.

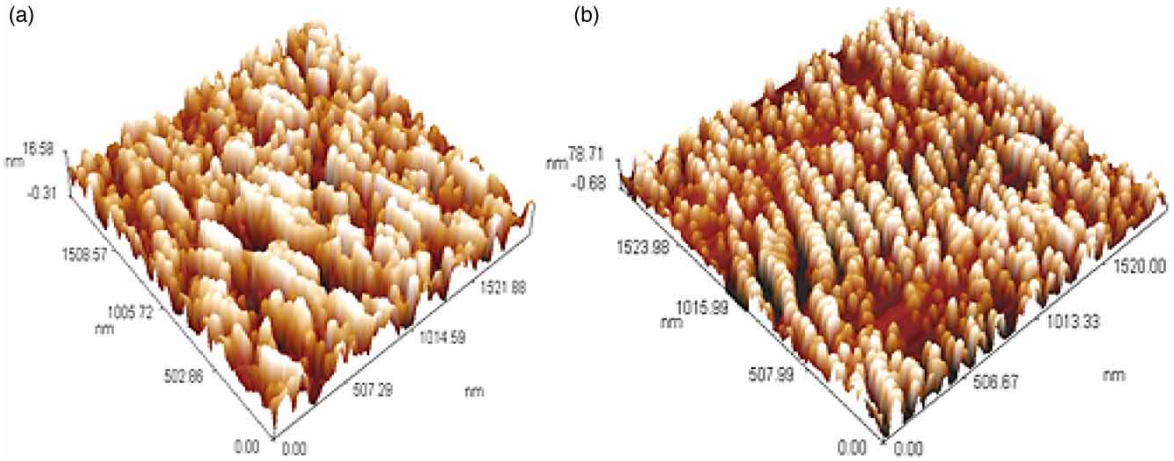

Figure 3 | SPM for SAC: (a) before MBD biosorption, (b) after MBD biosorption.

Table 3 | Characteristics of SAC before and after MBD biosorption using the SPM technique

Character	Before	After
Roughness average, Sa (nm)	19.9	3.8
Surface skewness, Ssk	0.00378	0.2223
Ten point height, Sz (nm)	79.2	16.9
Surface area ratio, Sdr	147	4.06
Core roughness depth, Sk (nm)	69	13.4

3.2. Factors influential on the MBD elimination

3.2.1. Impact of pH of MBD solution

The pH of the MBD solution is the most crucial element determining the biosorption process when compared to all other parameters (Vijayalaks *et al.* 2019). MBD biosorption by SAC is quite sensitive to the pH of the solution. The biosorption of an adsorbent is influenced by the chemistry of the adsorbent surface, which may be altered by

altering the primary pH value. Figure 4 depicts the effects of pH on MBD biosorption. SAC's dye removal effectiveness peaks at pH 9, but no significant gains in adsorbent removal performance have been found above that pH; therefore, pH 9 is regarded to be the optimal pH for SAC. Other research findings have also been published related to this one (Mahmoudi *et al.* 2015). The fact that the surface of the biosorbent is positively charged at lower pH values explains the pH impact on MBD biosorption since the quantity of MBD biosorbed ions rises as the pH value increases.

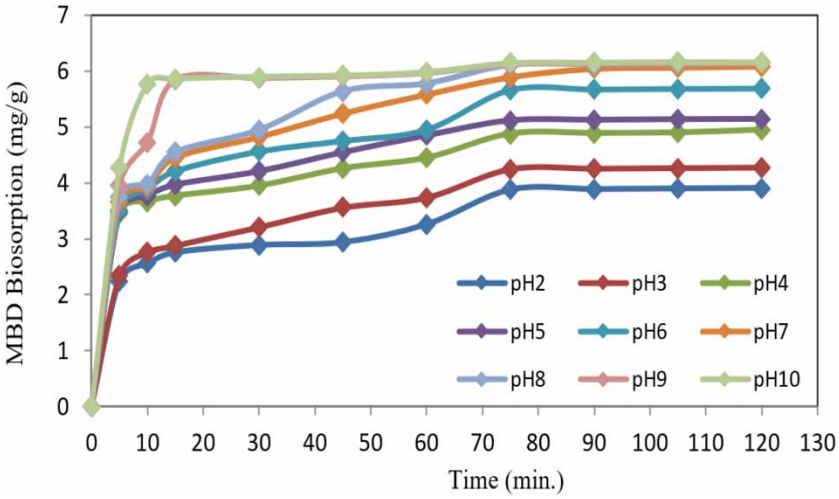

Figure 4 | The effect of initial pH in terms of contact time at various pHs on the biosorption efficiency of MBD at 50 mg/l and 250 rpm for 120 minutes using SAC with a mass of 0.8 g/100 ml.

The effect of pH on MBD removal was investigated based on the zero charge point (pH_{pzc}) of SAC. The pH at which the adsorbent's surface has a net zero charge is known as pH_{pzc}. SAC's pH_{pzc} was determined to be 4.4, as illustrated in Figure 5. This indicates that the SAC surface is protonated by H+ ion absorption at pHpzc, resulting in electrostatic repulsion with the cationic MBD. Furthermore, when $pH > pH_{pzc}$, the SAC surface has a negative charge, creating an electrostatic interaction with the cationic MBD. This clearly illustrates that the pH of the reaction mixture must be higher than pH_{pzc} for the cationic dye to biosorb (Shakoor & Nasar 2017).

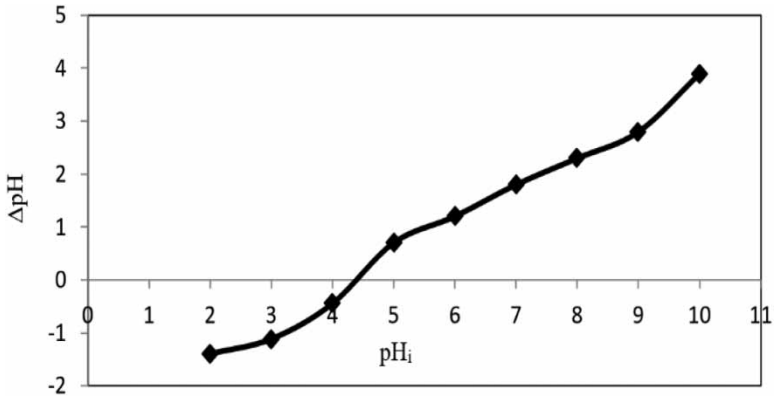

Figure 5 | Determination of point zero charge (pH_{pzc}) of SAC.

3.2.2. Impact of contact time

The effect of contact time on biosorption has been explored in the design of batch biosorption studies. Contact time between the adsorbent and the adsorbate is important in the biosorption process (Saleem *et al.* 2016). This period will be useful in determining the reasonableness of the binding and the best time for contaminant confiscation. Interaction time is another key parameter that impacts the biosorption technique's cost-effectiveness by controlling the biosorption operation's kinetics and supervising the motivational practice of a biosorbent for actual application (Mashkoor & Nasar 2019). Figure 6 depicts the impact of contact time on MBD removal by SAC as a biosorbent. It was discovered that increasing the contact duration (75 minutes) increased the removal

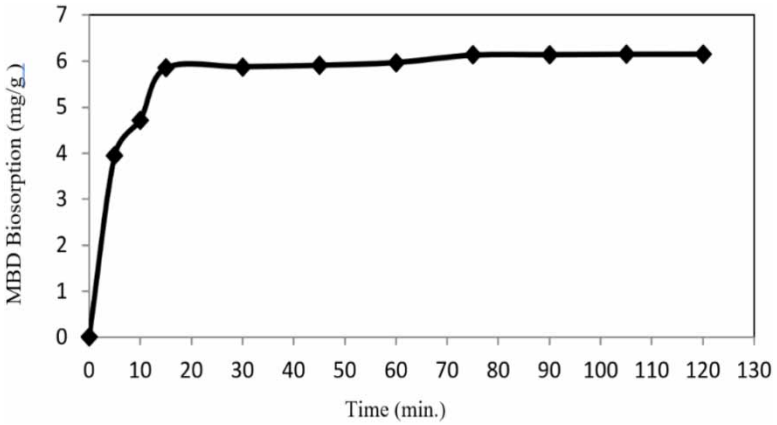

Figure 6 | Contact time effect on the removal efficiency of MBD onto SAC (dose = 0.8 g, initial MBD concentration = 50 mg/l, pH 9, 250 rpm for 120 min).

effectiveness, which remained constant in the 75–120 minutes range, which corresponded to 100% biosorption of the biosorbent. After that, the best time of 75 minutes was chosen for future investigation. It means that the elimination rate slows with time, and finally, a saturation level is reached (ElSayed 2018).

3.2.3. Impact of biosorbent dose

To find out how the biosorbent dosage affects biosorption capacity and MBD removal performance in the aqueous medium, SAC biosorbent dosages varied from 0.1 to 1.5 mg/100 ml, with an initial MBD concentration of 50 mg/l. In terms of biosorbent dosage, Figure 7 depicts MBD ions' percent removal and absorption. The removal effectiveness of MBD improved considerably from 85.92 to 98.68 percent when the dosage of biosorbent increased from 0.1 to 0.8 g, as shown in Figure 7. Further increasing the biosorbent dose over 0.8 g does not result in a significant improvement in MBD biosorption; hence the optimum SAC quantity was determined to be 0.8 g/100 ml. This periodic rise in removal effectiveness can be accompanied by an increase in the accessibility of additional active adsorbent sites for MBD biosorption with an increase in the SAC dosage. However, it is worth noting that biosorption ability has followed a remarkable decline pattern in biosorption capacity for SAC from 42.96 to 3.31 mg g^{-1} with a rise in biosorbent dose from 0.1 to 1.5 g/100 ml (Mashkoor & Nasar 2020). This might be because increasing the SAC amount increases the sorbent's interactions, such as

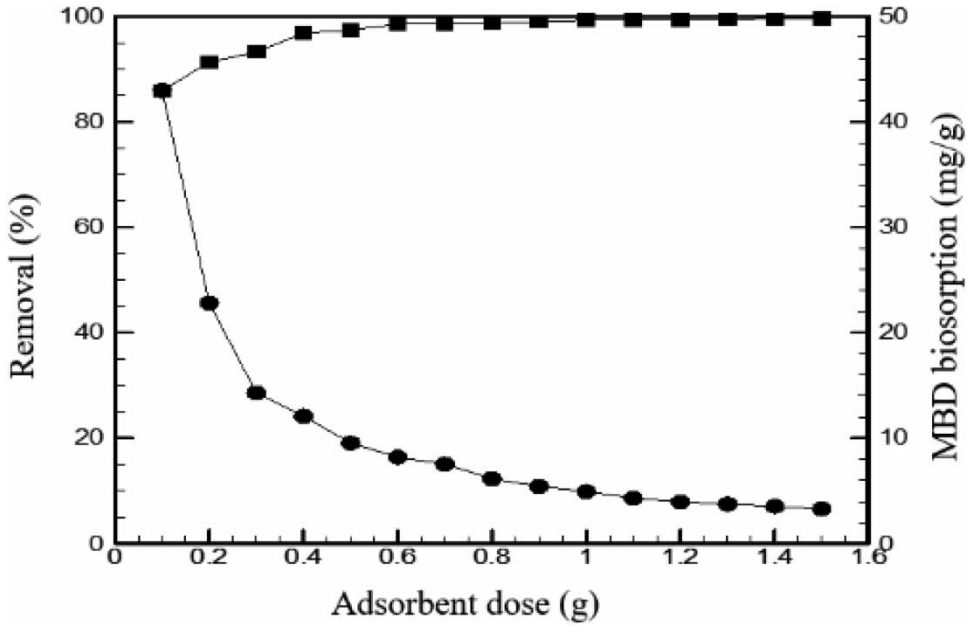

Figure 7 | Percentage removal and uptake of MBD ions in terms of biosorbent dose with initial dye concentration = 50 mg/L, pH9, 250 rpm using SAC with a contact time of 75 min.

accumulation, resulting in a considerable decrease in the sorbent's total surface area and, as a result, a decrease in its biosorption capacity (Ahmed *et al.* 2020).

3.2.4. Impact of initial MBD concentration

In biosorption experiments, the initial dye concentration is a critical element. The effect of the main concentration of MBD solution (10–100 mg/l) on removal efficiency and biosorption capacity in this sample is shown in Figure 8. As MBD strength grew from 10 to 100 mg/l, the efficacy of dye removal decreased, with a drop in the range of 100–96.8%. On the other hand, the biomass removal potential rose in direct proportion to the starting concentration of MBD solution. The absorption rose from 1.25–12.1 mg/g when the MBD concentration rose from 10 to 100 mg/l. The clearance effectiveness was also decreased as the dye concentration was increased in several tests. As the MBD strength increases, the number of active removal sites on the biomass surface decreases, and there are no more areas to adsorb dye onto SAC (Geetha *et al.* 2015). In other investigations, biomass adsorption increased with increasing starting dye concentrations. This may be related to the increased driving force (Zango 2018).

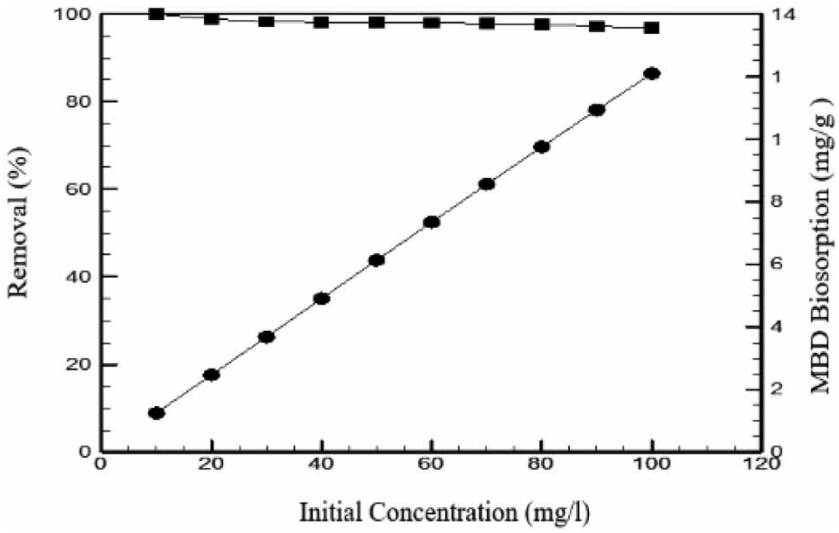

Figure 8 | Percentage removal and uptake of MBD ions as a function of MBD concentration (pH 9, 250 rpm): S AC with dose = 0.8 g/100 ml and contact time = 75 min.

4. MATHEMATICAL SIMULATION

4.1. Biosorption isotherm studies

The data of MBD biosorption onto SAC at equilibrium was examined using two commonly used isothermal simulations to describe the interaction between the biosorbent and the adsorbate, with R^2 and SE being used to assess the consistency of the fitting.

4.1.1. Langmuir isotherm

The Langmuir isothermal model assumes that monolayer adsorption occurs, that all adsorption sites at the adsorbent are structurally similar, and that adsorbed molecules at neighbouring sites do not interact (Gimbert *et al.* 2008). The adsorbent has limited adsorption ability, beyond which no further adsorption can occur when a molecule filled a site and reached equilibrium saturation (Langmuir 1918).

The linear mathematical formulation of the Langmuir isotherm is:

$$C_e/q_e = (1/(q_m * K_L)) + ((1/q_m) * C_e) \quad (3)$$

where C_e refers to the equilibrium strength (mg/l) and q_e is the quantity of absorbed species per quantity of biosorbent (mg/g), whereas K_L (l/mg) and q_m(mg/g) are the Langmuir measurements related to the affinity and maximum ability of biosorption, respectively. The *Ce/qe* vs C_e plot should produce a straight line with a slope ($1/q_m$) and interrupt ($1/q_m\ K_L$), as shown in Figure 9. The q_m and K_L values derived from the slope and intercept

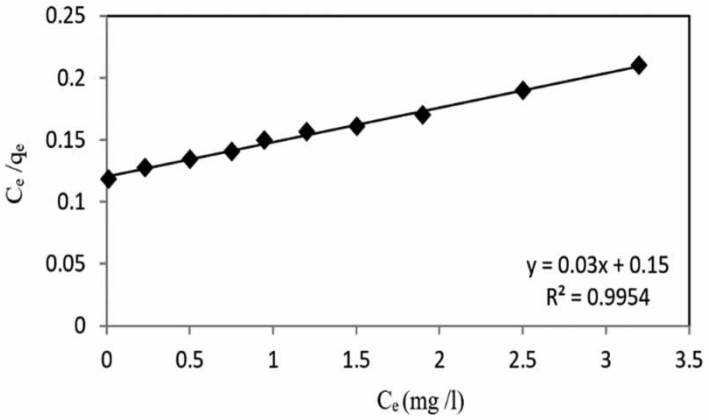

Figure 9 | Linearised model of MBD removal using SAC by Langmuir isotherm.

of the linear plot are shown in Table 4. The greater R^2 (0.9954) indicates that the Langmuir isothermal model is a good simulation for MBD equilibrium biosorption employing SAC, according to the researchers. The important representation of the Langmuir isotherm will be a unitless constant called the separation factor, R_L, given by Equation (4).

$$R_L = 1/(1 + K_L C_o) \tag{4}$$

Table 4 | Constants of biosorption isotherm for MBD using SAC

Langmuir (95% Confidence level)		**Freundlich (95% Confidence level)**	
q_m (mg/g)	33.34	K_F (mg/g) $(l/mg)^{1/n}$	6.94
K_L (l/mg)	0.2	1/n	0.39
R^2	0.9954	R^2	0.9785
S. E.	0.00204	S.E.	0.04522
R_L	(0.0476 – 0.3334)	Equation	$q_e = 6.94C_e^{0.39}$
Equation	$q_e = 6.67\ C_e/1 + 0.2\ C_e$		

The isothermal version of R_L might be unfavourable ($R_L > 1$), linear ($R_L = 1$), favourable ($0 < R_L < 1$), or irreversible ($R_L = 0$) (Dargo *et al.* 2014). From the graph in Figure 10, the Langmuir variable K_L was calculated to be 0.2, and the *qm* associated with biosorption capacity was calculated to be 33.34 mg/g. Under the aforementioned

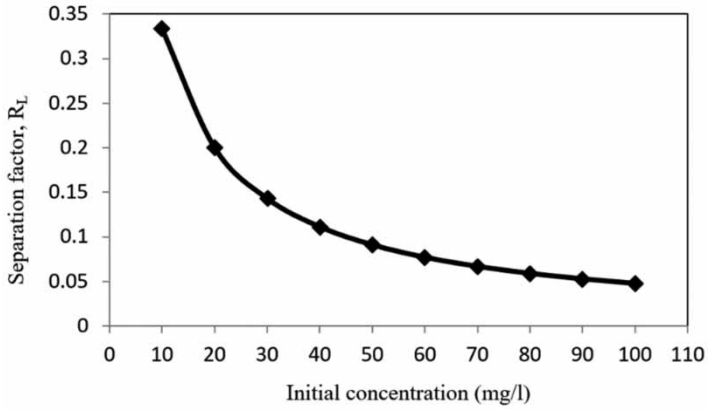

Figure 10 | Values of Separation Factor, R_L for Biosorption of MBD onto SAC.

experiment circumstances, R_L was also discovered to reflect the Langmuir isotherm applicability within the range of (0.0476–0.3333), as shown in Figure 10.

4.1.2. Freundlich isotherm

This practical isotherm model is also utilised to characterise the interaction between adsorbed molecules on various surfaces of non-identical sites and multi-layer adsorption with diverse energies. It is not limited to the monolayer formation of sorbate molecules on the biosorbent (Ho 2006; Alquzweeni *et al.* 2021). The well-known linear mathematical form indicated by the equation is the Freundlich isotherm:

$$\text{Log } q_e = \log K_F + 1/n \log C_e \tag{5}$$

The Freundlich isothermal constants for uptake and surface heterogeneity are K_F (mg/g) (l/mg)1/n and 1/n, respectively (Alquzweeni & Faisal 2020). The slope and intercept of the log q_e vs log C_e graph in Figure 11 may be used to compute the n and K_F values, which are then arranged in Table 4. The component (1/n) is a function of the sorbent surface's heterogeneity, and as 1/n approaches zero, it changes more heterogeneously.

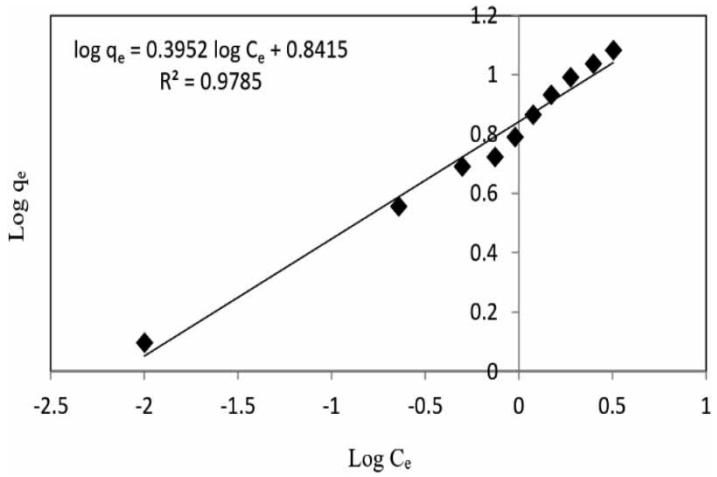

Figure 11 | Linearized Model of MBD Removal Using SAC by Freundlich Isotherm.

The ability of SAC to absorb MBD was compared to that of other biosorbents. The largest quantity of sorbed MBD was 34.33 mg/g. In addition, SAC had a higher adsorption capacity than the other biosorbents examined, as seen in Table 5 for MBD.

Table 5 | Comparison of the Langmuir uptake (q_m, mg.g^{-1}) with other biosorbents to remove MBD

Adsorbent	q_m (mg g^{-1})	Reference
Water hyacinth root	8.04	Soni *et al.* (2012)
Wild carrot	21	Swamy *et al.* (2017)
Delonix regia pods	23.3	Ho *et al.* (2009)
Defattedalgal biomass	7.8	Guarin *et al.* (2018)
Natural plant (Schanginia/sp.)	**33.34**	**The present study**

Figure 12 shows the comparisons of the MBD uptake potential between experimental data and those obtained using the Langmuir and Freundlich representations. The Langmuir model, which has a high R^2 and a low standard error (SE) value, better simulates the experimental data.

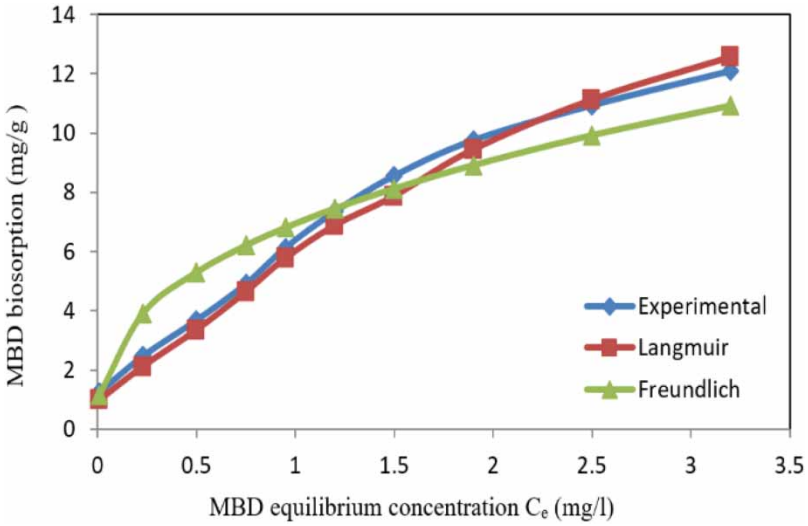

Figure 12 | Comparison of experimental and calculated data by Langmuir and Freundlich Equilibrium isotherm models.

5. CONCLUSIONS

Naturally occurring plant-based activated carbon was employed as a low-cost resource to remove MBD from aqueous solutions. S_{BET}, FTIR, SEM, and SPM examinations were used to characterise the surface of SAC before and after MBD removal. For biosorption tests, several factors such as the initial pH, agitation time, SAC mass, and initial MBD strength were studied. The Langmuir isotherm model was used to predict the SAC equilibrium biosorption of MBD, which resulted in a homogenous monolayer coating of MBD on the SAC surface. The maximal biosorption capacity was observed to be 33.34 mg/g. The MBD biosorption capability of SAC is greater than that of other agricultural biomass, and it may be easily manufactured without any chemical treatment.

For future studies, the new adsorbent could be applied to remove other pollutants, such as heavy metals and other types of dyes.

DATA AVAILABILITY STATEMENT

Data cannot be made publicly available; readers should contact the corresponding author for details.

REFERENCES

Abdulhadi, B. 2022 *Enhancing the Removal of Refractory Pollutants From Water Using Microwave-Electrocoagulation System*. Liverpool John Moores University, Liverpool, UK.

Abdulhadi, B., Kot, P., Hashim, K., Shaw, A., Muradov, M. & Al-Khaddar, R. 2021 Continuous-flow electrocoagulation (EC) process for iron removal from water: experimental, statistical and economic study. *Science of the Total Environment* **760**(2), 1–16.

Abdulredha, M., Rafid, A., Jordan, D. & Hashim, K. 2017 The development of a waste management system in Kerbala during major pilgrimage events: determination of solid waste composition. *Procedia Engineering* **196**, 779–784.

Ahmed, M., Mashkoor, F. & Nasar, A. 2020 Development, characterization, and utilization of magnetized orange peel waste as a novel adsorbent for the confiscation of crystal violet dye from aqueous solution. *Groundwater for Sustainable Development* **10**, 100322.

Albadarin, A. B., Mo, J., Glocheux, Y., Allen, S., Walker, G. & Mangwandi, C. 2014 Preliminary investigation of mixed adsorbents for the removal of copper and methylene blue from aqueous solutions. *Chemical Engineering Journal* **255**, 525–534.

Al-Hashimi, O., Hashim, K., Loffill, E., Marolt Čebašek, T., Nakouti, I., Faisal, A. A. & Al-Ansari, N. 2021 A comprehensive review for groundwater contamination and remediation: occurrence, migration and adsorption modelling. *Molecules* **26**(19), 5913.

Alquzweeni, S. & Faisal, A. 2020 Removal of lead ions from aqueous solution using granular iron slag byproduct as permeable reactive barrier. *The Iraqi Journal of Agricultural Science* **51**(2), 723–733.

Alquzweeni, S. S., Hassan, A. A. & Alkizwini, R. S. 2021 A novel application of building demolition waste for removal benzene from aqueous solutions. *Przegląd Naukowy Inżynieria I Kształtowanie Środowiska* **30**, 86–97.

Al-Sareji, O. J., Grmasha, R. A., Salman, J. M., Idowu, I. & Hashim, K. S. 2021 Street dust contamination by heavy metals in Babylon governorate, Iraq. *Journal of Engineering Science and Technology* **16**(1), 3528–3546.

Ansari, S. A., Khan, F. & Ahmad, A. 2016 Cauliflower leave, an agricultural waste biomass adsorbent, and Its application for the removal of MB dye from aqueous solution: equilibrium, kinetics, and thermodynamic studies. *International Journal of Analytical Chemistry* **2016**, 8252354.

Arab, M., Faramarz, M. G. & Hashim, K. 2022 Applications of computational and statistical models for optimizing the electrochemical removal of cephalexin antibiotic from water. *Water* **14**(3), 344–359.

Chen, H., Wang, X., Li, J. & Wang, X. 2015 Cotton derived carbonaceous aerogels for the efficient removal of organic pollutants and heavy metal ions. *Journal of Materials Chemistry A* **3**(11), 6073–6081.

Chung, K.-T. 2016 Azo dyes and human health: a review. *Journal of Environmental Science and Health, Part C* **34**(4), 233–261.

Dargo, H., Gabbiye, N. & Ayalew, A. 2014 Removal of methylene blue dye from textile wastewater using activated carbon prepared from rice husk. *International Journal of Innovation and Scientific Research* **9**(2), 317–325.

Das, R., Mukherjee, A., Sinha, I., Roy, K. & Dutta, B. K. 2020 Synthesis of potential bio-adsorbent from Indian Neem leaves (Azadirachta indica) and its optimization for malachite green dye removal from industrial wastes using response surface methodology: kinetics, isotherms and thermodynamic studies. *Applied Water Science* **10**(5), 1–18.

Dias, J. M., Alvim-Ferraz, M. C., Almeida, M. F., Rivera-Utrilla, J. & Sánchez-Polo, M. 2007 Waste materials for activated carbon preparation and its use in aqueous-phase treatment: a review. *Journal of Environmental Management* **85**(4), 833–846.

ElSayed, E. E. 2018 Natural diatomite as an effective adsorbent for heavy metals in water and wastewater treatment (a batch study). *Water Science* **32**(1), 32–43.

Emamjomeh, M. M., Kakavand, S., Jamali, H. A., Alizadeh, S. M., Safdari, M., Mousavi, S. E. S., Hashim, K. S. & Mousazade, M. 2020 The treatment of printing and packaging wastewater by electrocoagulation–flotation: the simultaneous efficacy of critical parameters and economics. *Desalination and Water Treatment* **205**, 161–174.

Etim, E. U. 2019 Removal of methyl blue dye from aqueous solution by adsorption unto ground nut waste. *Biomedical Journal of Scientific & Technical Research* **15**(3), 11365–11371.

Geetha, P., Latha, M. & Koshy, M. 2015 Biosorption of malachite green dye from aqueous solution by calcium alginate nanoparticles: equilibrium study. *Journal of Molecular Liquids* **212**, 723–730.

Georgin, J., Dotto, G. L., Mazutti, M. A. & Foletto, E. L. 2016 Preparation of activated carbon from peanut shell by conventional pyrolysis and microwave irradiation-pyrolysis to remove organic dyes from aqueous solutions. *Journal of Environmental Chemical Engineering* **4**(1), 266–275.

Giannakoudakis, D. A., Hosseini-Bandegharaei, A., Tsafrakidou, P., Triantafyllidis, K. S., Kornaros, M. & Anastopoulos, I. 2018 Aloe vera waste biomass-based adsorbents for the removal of aquatic pollutants: a review. *Journal of Environmental Management* **227**, 354–364.

Gimbert, F., Morin-Crini, N., Renault, F., Badot, P.-M. & Crini, G. 2008 Adsorption isotherm models for dye removal by cationized starch-based material in a single component system: error analysis. *Journal of Hazardous Materials* **157**(1), 34–46.

Grmasha, R. A., Al-Seady, M. A., Al-Aaraji, N. A.-H. & Abduljalil, H. M. 2021 Investigation adsorption mechanism of methane gas in graphene and copper doped nano-ribbon using density function theory. *Journal of Physics: Conference Series, IOP Publishing* **032099**, 1–7.

Guarin, J. R., Moreno-Pirajan, J. C. & Giraldo, L. 2018 Kinetic study of the bioadsorption of methylene blue on the surface of the biomass obtained from the Algae D. Antarctica. *Journal of Chemistry* **2018**, 1–12.

Hashim, K. S., Hussein, A. H., Zubaidi, S. L., Kot, P., Kraidi, L., Alkhaddar, R., Shaw, A. & Alwash, R. 2019 Effect of initial pH value on the removal of reactive black dye from water by electrocoagulation (EC) method. In: *2nd International Scientific Conference*. Al-Qadisiyah University, Iraq, pp. 12–22.

Hashim, K. S., Ewadh, H. M., Muhsin, A. A., Zubaidi, S. L., Kot, P., Muradov, M., Aljefery, M. & Al-Khaddar, R. 2021a Phosphate removal from water using bottom ash: adsorption performance, coexisting anions and modelling studies. *Water Science and Technology* **83**(1), 77–89.

Hashim, K. S., Shaw, A., AlKhaddar, R., Kot, P. & Al-Shamma'a, A. 2021b Water purification from metal ions in the presence of organic matter using electromagnetic radiation-assisted treatment. *Journal of Cleaner Production* **280**(2), 1–17.

Ho, Y.-S. 2006 Isotherms for the sorption of lead onto peat: comparison of linear and non-linear methods. *Polish Journal of Environmental Studies* **15**, 1.

Ho, Y.-S., Malarvizhi, R. & Sulochana, N. 2009 Equilibrium isotherm studies of methylene blue adsorption onto activated carbon prepared from Delonix regia pods. *Journal of Environmental Protection Science* **3**(2), 111–116.

Jabar, J. M., Odusote, Y. A., Alabi, K. A. & Ahmed, I. B. 2020 Kinetics and mechanisms of Congo-red dye removal from aqueous solution using activated Moringa oleifera seed coat as adsorbent. *Applied Water Science* **10**(6), 1–11.

Jawad, A. H., Ngoh, Y. & Radzun, K. A. 2018 Utilization of watermelon (Citrullus lanatus) rinds as a natural low-cost biosorbent for adsorption of methylene blue: kinetic, equilibrium and thermodynamic studies. *Journal of Taibah University for Science* **12**(4), 371–381.

Jawad, A. H., Ismail, K., Ishak, M. A. M. & Wilson, L. D. 2019 Conversion of Malaysian low-rank coal to mesoporous activated carbon: structure characterization and adsorption properties. *Chinese Journal of Chemical Engineering* **27**(7), 1716–1727.

Kanthasamy, S., Hadibarata, T., Hidayat, T., Alamri, S. A. & Al-Ghamdi, A. A. 2020 Adsorption of azo and anthraquinone dye by using watermelon peel powder and corn peel powder: equilibrium and kinetic studies. *Biointerface Research in Applied Chemistry* **10**(1), 4706–4713.

Karaghool, H. A. K., Hashim, K., Kot, P. & Muradov, M. 2022 Preliminary studies of methylene blue remotion from aqueous solutions by ocimum basilicum. *Environments* **9**(2), 1–17.

Langmuir, I. 1918 The adsorption of gases on plane surfaces of glass, mica and platinum. *Journal of the American Chemical Society* **40**(9), 1361–1403.

Latif, S., Rehman, R., Imran, M., Iqbal, S., Kanwal, A. & Mitu, L. 2019 Removal of acidic dyes from aqueous media using Citrullus lanatus peels: an agrowaste-based adsorbent for environmental safety. *Journal of Chemistry* **2019**, 20–29.

Mahamad, M. N., Zaini, M. A. A. & Zakaria, Z. A. 2015 Preparation and characterization of activated carbon from pineapple waste biomass for dye removal. *International Biodeterioration & Biodegradation* **102**, 274–280.

Mahmoudi, K., Hosni, K., Hamdi, N. & Srasra, E. 2015 Kinetics and equilibrium studies on removal of methylene blue and methyl orange by adsorption onto activated carbon prepared from date pits-A comparative study. *Korean Journal of Chemical Engineering* **32**(2), 274–283.

Mashkoor, F. & Nasar, A. 2019 Preparation, characterization and adsorption studies of the chemically modified Luffa aegyptica peel as a potential adsorbent for the removal of malachite green from aqueous solution. *Journal of Molecular Liquids* **274**, 315–327.

Mashkoor, F. & Nasar, A. 2020 Magnetized Tectona grandis sawdust as a novel adsorbent: preparation, characterization, and utilization for the removal of methylene blue from aqueous solution. *Cellulose* **27**(5), 2613–2635.

Mohseni-Bandpi, A., Al-Musawi, T. J., Ghahramani, E., Zarrabi, M., Mohebi, S. & Vahed, S. A. 2016 Improvement of zeolite adsorption capacity for cephalexin by coating with magnetic Fe3O4 nanoparticles. *Journal of Molecular Liquids* **218**, 615–624.

Oliva, J., Martinez, A., Oliva, A., Garcia, C., Martinez-Luevanos, A., Garcia-Lobato, M., Ochoa-Valiente, R. & Berlanga, A. 2018 Flexible graphene composites for removal of methylene blue dye-contaminant from water. *Applied Surface Science* **436**, 739–746.

Omran, I. I., Al-Saati, N. H., Hashim, K. S., Al-Saati, Z. N., Patryk, K., Khaddar, R. A., Al-Jumeily, D., Shaw, A., Ruddock, F. & Aljefery, M. 2019 Assessment of heavy metal pollution in the Great Al-Mussaib irrigation channel. *Desalination and Water Treatment* **168**, 165–174.

Rao, H. J. 2021 Characterization studies on adsorption of lead and cadmium using activated carbon prepared from waste tyres. *Nature Environment & Pollution Technology* **20**(2), 561–568.

Salah, Z. L., Gharghan, S. K., Dooley, J., Alkhaddar, R. M. & Abdellatif, M. 2018 Short-term urban water demand prediction considering weather factors. *Water Resources Management* **32**(14), 4527–4542.

Salah, Z., Hashim, K., Ethaib, S., Al-Bdairi, N. S. S., Al-Bugharbee, H. & Gharghan, S. K. 2022 A novel methodology to predict monthly municipal water demand based on weather variables scenario. *Journal of King Saud University-Engineering Sciences* **34**(3), 163–169.

Saleem, M., Wongsrisujarit, N. & Boonyarattanakalin, S. 2016 Removal of nickel (II) ion by adsorption on coconut copra meal biosorbent. *Desalination and Water Treatment* **57**(12), 5623–5635.

Sever, B., Çiftçi, G. A., Özdemir, A. & Altıntop, M. D. 2019 Design, synthesis and in vitro evaluation of new thiosemicarbazone derivatives as potential anticancer agents. *Journal of Chemistry* **7**, 1–7.

Shakoor, S. & Nasar, A. 2017 Adsorptive treatment of hazardous methylene blue dye from artificially contaminated water using cucumis sativus peel waste as a low-cost adsorbent. *Groundwater for Sustainable Development* **5**, 152–159.

Sharma, S. & Kaur, A. 2018 Various methods for removal of dyes from industrial effluents-a review. *Indian Journal of Science and Technology* **11**(1), 20–41

Silva, F., Nascimento, L., Brito, M., da Silva, K., Paschoal, W. & Fujiyama, R. 2019 Biosorption of methylene blue dye using natural biosorbents made from weeds. *Materials* **12**(15), 2486.

Sivarajasekar, N. & Baskar, R. 2015 Agriculture waste biomass valorisation for cationic dyes sequestration: a concise review. *Journal of Chemical and Pharmaceutical Research* **7**(9), 737–748.

Soni, M., Sharma, A. K., Srivastava, J. K. & Yadav, J. 2012 Adsorptive removal of methylene blue dye from an aqueous solution using water hyacinth root powder as a low cost adsorbent. *International Journal of Chemical Sciences and Applications* **3**(3), 338–345.

Soonmin, H. 2018 Removal of dye by adsorption onto activated carbons. *Eurasian Journal of Analytical Chemistry* **13**(4), 332–338.

Swamy, M. M., Nagabhushana, B., Krishna, R. H., Kottam, N., Raveendra, R. & Prashanth, P. 2017 Fast adsorptive removal of methylene blue dye from aqueous solution onto a wild carrot flower activated carbon: isotherms and kinetics studies. *Water Treat* **71**, 399–405.

Tahir, H., Sultan, M., Akhtar, N., Hameed, U. & Abid, T. 2016 Application of natural and modified sugar cane bagasse for the removal of dye from aqueous solution. *Journal of Saudi Chemical Society* **20**, S115–SS21.

Teka, T. & Enyew, S. 2014 Study on effect of different parameters on adsorption efficiency of low cost activated orange peels for the removal of methylene blue dye. *International Journal of Innovation and Scientific Research* **8**(1), 106–111.

Vijayalaks, G., Ramkumar, B. & Mohan, S. C. 2019 Isotherm and kinetic studies of methylene blue adsorption using activated carbon prepared from teak wood waste biomass. *Journal of Applied Sciences* **19**(9), 827–836.

Wong, K. T., Eu, N. C., Ibrahim, S., Kim, H., Yoon, Y. & Jang, M. 2016 Recyclable magnetite-loaded palm shell-waste based activated carbon for the effective removal of methylene blue from aqueous solution. *Journal of Cleaner Production* **115**, 337–342.

Yagub, M. T., Sen, T. K., Afroze, S. & Ang, H. M. 2014 Dye and its removal from aqueous solution by adsorption: a review. *Advances in Colloid and Interface Science* **209**, 172–184.

Zango, Z. U. 2018 Cationic dyes removal using low-cost banana peel biosorbent. *American Journal of Materials Science* **8**(2), 32–38.

Zhang, J., Landry, M. P., Barone, P. W., Kim, J.-H., Lin, S., Ulissi, Z. W., Lin, D., Mu, B., Boghossian, A. A. & Hilmer, A. J. 2013 Molecular recognition using corona phase complexes made of synthetic polymers adsorbed on carbon nanotubes. *Nature Nanotechnology* **8**(12), 959–968.

First received 12 February 2022; accepted in revised form 13 April 2022. Available online 27 April 2022